Lithos 390–391 (2021) 106114

Contents lists available at ScienceDirect

Lithos

journal homepage: www.elsevier.com/locate/lithos

Research Article

Prolonged basaltic magmatism and short-lived magmatic sulfide mineralization in orogenic belts

Xie-Yan Song [a,*], Yu-Feng Deng [b], Wei Xie [c], Jun-Nian Yi [d], Bin Fu [e], Lie-Meng Chen [a], Song-Yue Yu [a], Wen-Qin Zheng [a], Qing-Lin Liang [a]

[a] State Key Laboratory of Ore Deposit Geochemistry, Institute of Geochemistry, Chinese Academy of Sciences, Guiyang 550081, PR China
[b] Ore Deposit and Exploration Center (ODEC), Hefei University of Technology, Hefei, Anhui 230009, PR China
[c] College of Oceanography, Hohai University, Nanjing 210098, PR China
[d] Institute for Ecological Civilization of Karst Area, Guizhou Normal University, Guiyang 550001, PR China
[e] Research School of Earth Sciences, The Australian National University, Canberra, ACT 2600, Australia

ARTICLE INFO

Article history:
Received 9 December 2020
Received in revised form 4 March 2021
Accepted 7 March 2021
Available online 16 March 2021

Keywords:
Short-lived magmatic sulfide mineralization
Orogenic belt
Ni-Cu sulfide deposit
Collision
Slab break-off
Melting of asthenosphere

ABSTRACT

Economically important Ni-Cu sulfide deposits occur in orogenic belts worldwide. However, the duration of timing and geological processes critical for generation of high-Mg basaltic magma and Ni-Cu sulfide mineralization during orogeny have not been well addressed. Here, we report a detailed geochronological study on the Huangshan-Jingerquan Ni-Cu metallogenic belt, NW China. The complexes were regarded as the results of a prolonged basaltic magmatism from 380 Ma to 270 Ma according to previous zircon U-Pb ages. Most of the zircons for the previous age dating were separated from mafic facies and only a few from ultramafic rocks. However, the Ni-Cu sulfide ore bodies are mostly hosted within the ultramafic facies. Thus, there are debates on tectonic setting of the magmatism associated with the Ni-Cu sulfide mineralization. In this study, the zircons separated from the sulfide-mineralized mafic/ultramafic facies of eleven complexes display U-Pb ages ranging from 285 to 280 Ma, indicating a short-lived high-Mg basaltic magmatism associated with the Ni-Cu mineralization. It is likely that the olivine-free gabbros formed in 380–300 Ma and 280–270 Ma occurred in subduction and post-collisional periods, respectively. Collision combined with regional strike-slip shearing at the latest Carboniferous induced slab break-off and asthenosphere upwelling in early Permian. Decompression melting of the upwelling asthenosphere was extensively intensified by addition of water released from the broken slab and generated voluminous high-Mg basaltic magma beneficial to the short-lived Ni-Cu sulfide mineralization in 285–280 Ma. The regional strike-slip shearing created fracture networks as pathways for magma ascending. The sulfides carried by the ascending basaltic magma deposited in the fractures and magma chambers in different depths and produced the sulfide-mineralized dykes and complexes, respectively.

1. Introduction

Economic Ni-Cu sulfide deposits hosted by mafic-ultramafic complexes have been discovered in orogenic belts worldwide, such as the Aguablanca deposit in Spain (e.g., Piña et al., 2010), the Selebi-Phikwe belt in Botswana (Maier et al., 2008), the Kotalahti and Vammala belts in Finland (e.g., Barnes et al., 2009), and the Savannah Ni-Cu-Co Camp in Australia (Vaillant et al., 2020). In China, some large Ni-Cu sulfide deposits have been discovered in several orogenic belts: the giant Xiarihamu Ni-Co deposit in the East Kunlun Orogenic Belt, Tibet Plateau (Liu et al., 2018; Song et al., 2016, 2020 and references therein), the Lengshuiqing deposit along the western margin of the Yangzi Block (Yao et al., 2018), and the Huangshan-Jingerquan belt and the Hongqiling deposit, from west to east, along the southern margin of the Central Asian Orogenic Belt (abbreviated to CAOB in text below) (Li et al., 2019; Song et al., 2013; Wei et al., 2013). Of them, the Huangshan-Jingerquan Ni-Cu metallogenic belt contains ~1/3 Ni metal reserves of the magmatic sulfide deposits in the orogenic belts in China (~3.5 million tonnes Ni) (Table 1, Fig. 1). Both the Xiarihamu Ni-Co deposit (~157Mt@0.65 wt% Ni, 0.013 wt% Co) in the East Kunlun Orogenic Belt (China) and the Nova Ni-Cu-Co deposit (14.6Mt@2.2 wt % Ni, 0.9 wt% Cu, 0.08 wt% Co) in the Albany-Fraser Orogenic Belt (Australia) are the largest Ni deposits in the world (Li et al., 2015; Maier et al., 2016; Song et al., 2016) since the discovery of Voisey's Bay (Canada) and Nebo-Babel (Australia) (e.g., Godel et al., 2011; Ripley and Li, 2011; Seat et al., 2011). This has led to an aspiration of further mineral exploration for magmatic sulfide deposit in orogenic belts.

Although orogeny is one of the most common geological processes throughout the Earth's history, occurrences of Ni-Cu sulfide deposits

* Corresponding author.
E-mail address: songxieyan@vip.gyig.ac.cn (X.-Y. Song).

https://doi.org/10.1016/j.lithos.2021.106114
0024-4937/

Table 1
The mafic-ultramafic complexes in the Huangshan-Jingerquan belt.

Strata hosting the complex	Complex/deposit	Complex shape	Rock assemblage	Ore reserves /grades/annual output of ore	U-Pb age of zircon (Ma)	Number of sample in this study	Method of U-Pb measurement	Rock for zircon separation	Containing sulfides	References
Gandun Formation	Tudun	Oval	Peridotites and gabbros	5Mt/0.3% Ni, 0.2% Cu/mining stopped	282.8 ± 1.7	17TD-112	SHRIMP	Lherzolite	Yes	This study (Beijing)
					280.0 ± 3.0		SHRIMP	Gabbro	No	Song et al., 2013
	Erhongwa	Oval	Peridotites and gabbros	9Mt/0.2% Ni, 0.05% Cu/unmined	281.3 ± 3.5	17E-111	SHRIMP	Lherzolite	Yes	This study (Beijing)
					283.1 ± 1.5		LA-ICP-MS	Olivine gabbro	No	Sun et al., 2013a, 2013b
	Huangshan	Bean-pod	Peridotites and gabbros	75Mt/0.45% Ni, 0.23% Cu/1.32Mt (mining from 2008)	280.5 ± 1.9	HSX1	SHRIMP	Lherzolite	Yes	This study (ANU)
					283.0 ± 2.0	DHS17-24	SHRIMP	Basal gabbronorite	Yes	This study (Beijing)
					283.8 ± 3.4		SIMS	Gabbronorite	Yes	Qin et al., 2011
					284.5 ± 2.5		LA-ICP-MS	Gabbronorite	Yes	Gu et al., 2006
					269.0 ± 2.0		SHRIMP	Diorite	No	Zhou et al., 2004
	Huangshandong	Rhombus	Peridotites, gabbros, diorite	90Mt/0.4% Ni, 0.2% Cu/0.5Mt (mining from 2000)	284.2 ± 2.0	HSDD-02	LA-ICP-MS	Lherzolite	Yes	This study (Hefei)
					283.4 ± 3.0	16HSDD-02	SHRIMP	Olivine gabbro	Yes	This study (Beijing)
					282.7 ± 1.4	HSDD-01	LA-ICP-MS	Gabbronorite	Yes	This study (Hefei)
					281.4 ± 2.2		SIMS	Lherzolite	Yes	Mao et al., 2019
					280.3 ± 1.9		SIMS	Olivine gabbro	Yes	Mao et al., 2019
					274.0 ± 3.0		SHRIMP	Olivine-free gabbro	No	Han et al., 2004
Gandun Formation	Huangshandong	Rhombus	Peridotites, gabbros, diorite	90Mt/0.4% Ni, 0.2% Cu/0.32Mt (mining from 2000)	274.5 ± 3.6		LA-ICP-MS	Olivine-free gabbro	No	Wang et al., 2014
					271.2 ± 3.8		LA-ICP-MS	Olivine-free gabbro	No	
					268.2 ± 2.1		LA-ICP-MS	Olivine-free gabbro	No	
					267.0 ± 2.1		LA-ICP-MS	Olivine-free gabbro	No	
					277.0 ± 1.1		LA-ICP-MS	Olivine-free gabbro	No	Chen et al., 2013
	Huangshannan	Oval	Peridotites, gabbros, diorite	30Mt/0.4% Ni, 0.1% Cu/0.45Mt (mining from 2011)	284.1 ± 2.3	HSN1	SHRIMP	Lherzolite	Yes	This study (Beijing)
					279.2 ± 2.6	HSN1	SHRIMP	Lherzolite	Yes	This study (ANU)
					282.5 ± 1.4		SIMS	Gabbro	No	Zhao et al., 2015
					278.0 ± 2.0		SIMS	Gabbro	No	Mao et al., 2016
					270.0 ± 5.0		SHRIMP	Olivine-free gabbro	No	Song et al., 2013
	Hongliugou	Dyke-like	Peridotites and gabbros	Mineralization	281.4 ± 2.3	HLG-1	SHRIMP	Norite	No	This study (Beijing)
Wutongwozi Formation	Xiangshan	Dyke-like	Peridotites, gabbros, diorite	8Mt/0.5% Ni, 0.25% Cu/unmined	279.6 ± 1.1		SIMS	Gabbro	No	Han et al., 2010
					278.6 ± 1.8		SIMS	Ilmenite-bearing gabbro	No	Xiao et al., 2010
					283.2 ± 2.1		SIMS	Gabbro	No	Li et al., 2012
					285.0 ± 1.1		LA-ICP-MS	Gabbro	No	Chen et al., 2013
					280.1 ± 1.5		LA-ICP-MS	Gabbro	No	Shi et al., 2018
					279.2 ± 1.4		LA-ICP-MS	Ilmenite-bearing gabbro	No	
	Hongshigang	Oval	Peridotites, gabbros, diorite	Mineralization	280.0 ± 1.0		LA-ICP-MS	Gabbro	No	Shi et al., 2019
Wutongwozi Formation	Hongshigangbei	Oval	Gabbro, diorite	Mineralization	276.1 ± 5.4		LA-ICP-MS	Gabbro	No	Wang et al., 2019
	Jingerquanbei	Chain of small pods	Peridotites, gabbros, diorite	Mineralization	281.7 ± 2.5	JEB-1	SHRIMP	Lherzolite	Yes	This study (Beijing)
					316.0 ± 3.2	JEB-2	SHRIMP	Olivine-free gabbro	No	This study (Beijing)
	Hulu	Elongate lopolith	Peridotite, gabbro	16Mt/0.5% Ni, 0.25% Cu/0.11Mt (mining from 2004)	282.9 ± 1.8	HL18-A	SHRIMP	Websterite	Yes	This study (Beijing)
					282.3 ± 1.2		SIMS	Marginal gabbro	No	Han et al., 2013
					274.5 ± 3.9		LA-ICP-MS	Diorite	No	Sun et al., 2010
					381.6 ± 1.3		SIMS	Coarse-grained gabbro beneath websterite	No	Zhao et al., 2018
					377.0 ± 3.0		SIMS			
					388.6 ± 2.7		SIMS			
	Mati	Chain of small pods	Lherzolite	Mineralization	281.8 ± 2.2	MT18A	SHRIMP	Lherzolite	Yes	This study (ANU)
	Tulaergen	Dyke-like	Peridotites, gabbros, diorite	30Mt/0.45% Ni, 0.2% Cu/0.73Mt (mining from 2010)	281.0 ± 2.2	TLD19-1B	SHRIMP	Lherzolite	Yes	This study (Beijing)
					300.5 ± 3.2		SHRIMP	Olivine-free gabbro	No	San et al., 2010
					357.5 ± 2.5		SHRIMP	Olivine-free gabbro	No	
					351.0 ± 4.0		SHRIMP	Olivine-free gabbro	No	Jiao et al., 2013
	Xianshuiquan	Dyke-like	Gabbros	Mineralization	380.4 ± 3.3	TPD-6	SHRIMP	Olivine-free gabbro	No	This study (Beijing)

Most of the Ni-Cu sulfide deposits (Huangshan, Huangshandong, Huangshannan, Tudun, Hulu, Xiangshan, etc.) and mineralized mafic-ultramafic complexes were discovered in 1980's. The Tulaergen deposit was discovered in 2010 and the mineralization in the Dahuangshan, Jingerquanbei, and Hongshigang was newly discovered in recent years. All of the mines are underground. Many other references without age data cannot be cited due to space limitation. The zircons of the sample HSN1 from the Huangshannan complex were measured in Australian National University (ANU) and Beijing SHRIMP Centre (Beijing). Both laboratories gave the same age taking into account measurement error.

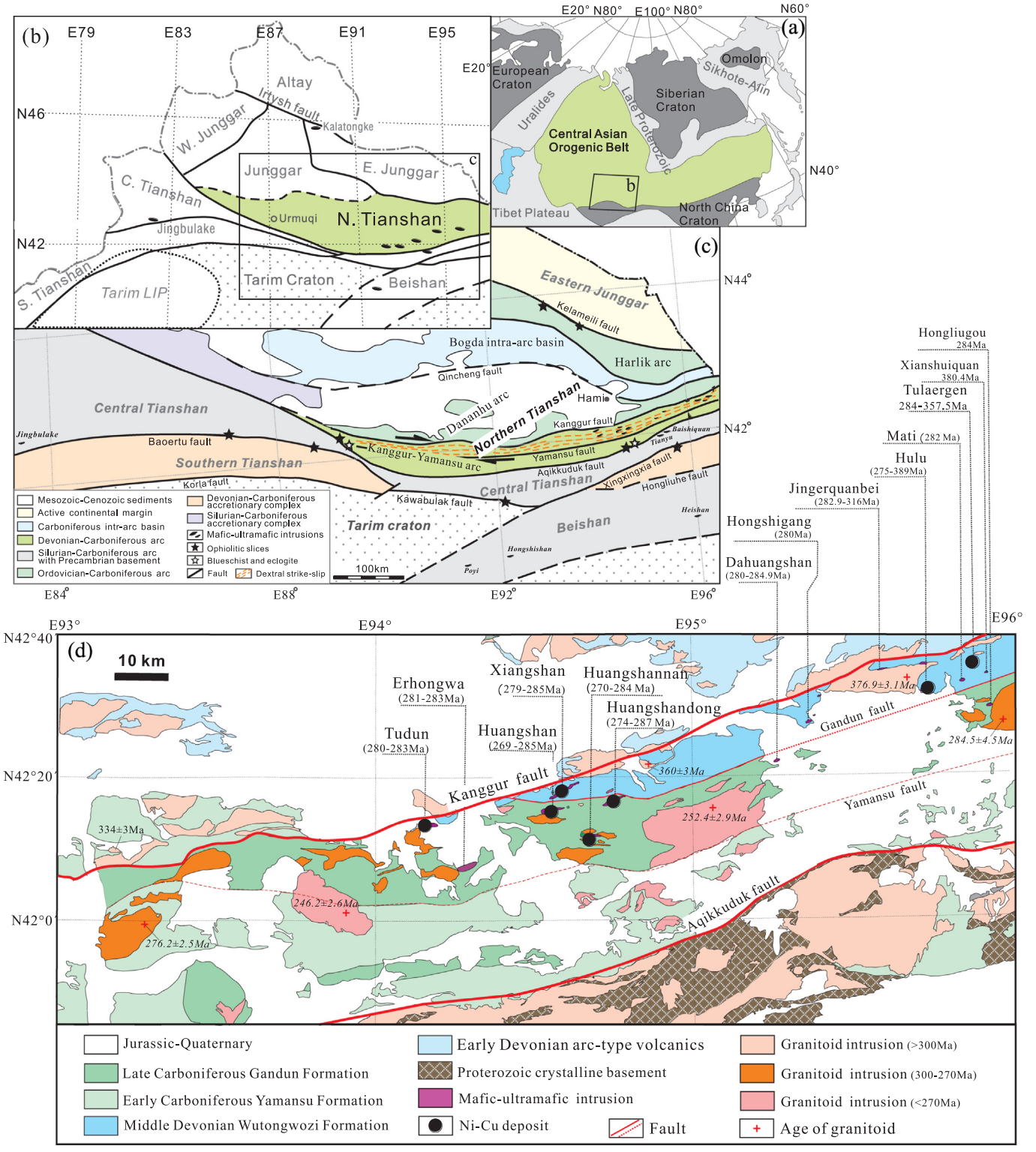

Fig. 1. (a) Location of the Central Asian Orogenic Belt (CAOB). (b) Tectonic domains at southern margin of CAOB in NW China. (c) The North Tianshan arc system is bounded by the Kelameili and Aqikkuduk faults and consists of the Harlik-Dananhu island arc in the north and the Kanggur-Yamansu arc in the south. (d) Simplified geological map of the Kanggur-Yamansu arc, the Huangshan-Jingerquan Ni-Cu metallogenic belt is located to the north of the Yamansu fault. Information is from Xiao et al. (2015), Song et al. (2013) and references therein, age data and detailed information are listed in Table 1.

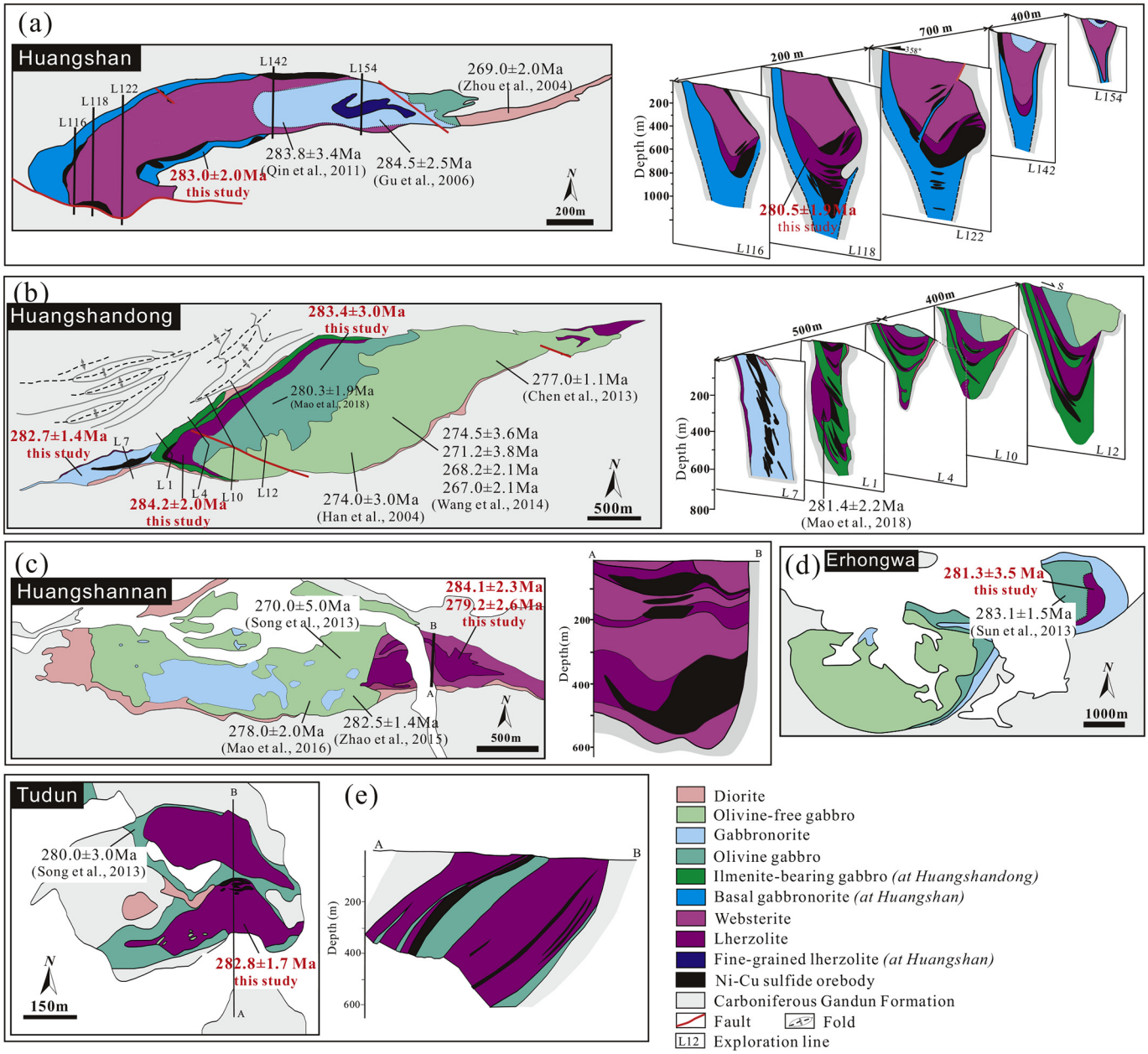

Fig. 2. The mafic-ultramafic complexes emplaced in the late Carboniferous Gandun Formation after Deng et al., 2014 and references therein. Geological maps and selected cross sections show the contact relationships among the mafic and ultramafic facies, locations of the Ni-Cu sulfide mineralization and age data of the bean-pod shaped Huangshan complex (a), the rhombic Huangshandong, Huangshannan and Erhongwa complexes (b, c, d), as well as oval Tudun complex (e).

are rare in most of the orogenic belts. During development of orogenic belts, basaltic magmatism can occur in subduction, collision and post-collision periods (e.g., Davies and von Blanckenburg, 1995; Freeburn et al., 2017). The related mafic-ultramafic intrusions are produced by complicated and prolonged processes of magma generation, emplacement and evolution in different periods, which are not fully understood. As a result, some fundamental questions on the formation of the Ni-Cu sulfide deposits hosted in the mafic-ultramafic complexes in orogenic belts still remain poorly constrained: (1) What are the critical processes for the generation of voluminous high-Mg basaltic magma beneficial to the formation of large deposit? (2) When is the optimal period for the extensive basaltic magmatism in geodynamic history of an orogenic belt? (3) What are the favorable structures for sulfide-bearing magma migration and sulfide accumulation?

Lithological relationships of the mafic-ultramafic complexes in the Huangshan-Jingerquan belt, particularly the sharp contacts between the sulfide-mineralized and sulfide-barren facies in the complexes, such as the Huangshan, Huangshandong, etc. (Figs. 2, 3, see descriptions below), cannot be interpreted merely by magmatic fractionation but reflect multiple magma emplacements (Deng et al., 2020; Zhou et al., 2004 and references therein). Recently published zircon U-Pb ages for the sulfide-barren gabbros of the complexes indicated a prolonged basaltic magmatism history (~267–380 Ma), whereas only a few U-Pb ages for the Ni-Cu sulfide-mineralized facies of the Huangshan and Huangshandong complexes range from 284.5 ± 2.5 to 280.3 ± 1.9 Ma (Table 1 with references). Thus, there are controversies on tectonic setting of the basaltic magmatism resulting in the Ni-Cu sulfide mineralization along the belt. The basaltic magmatism was attributed to

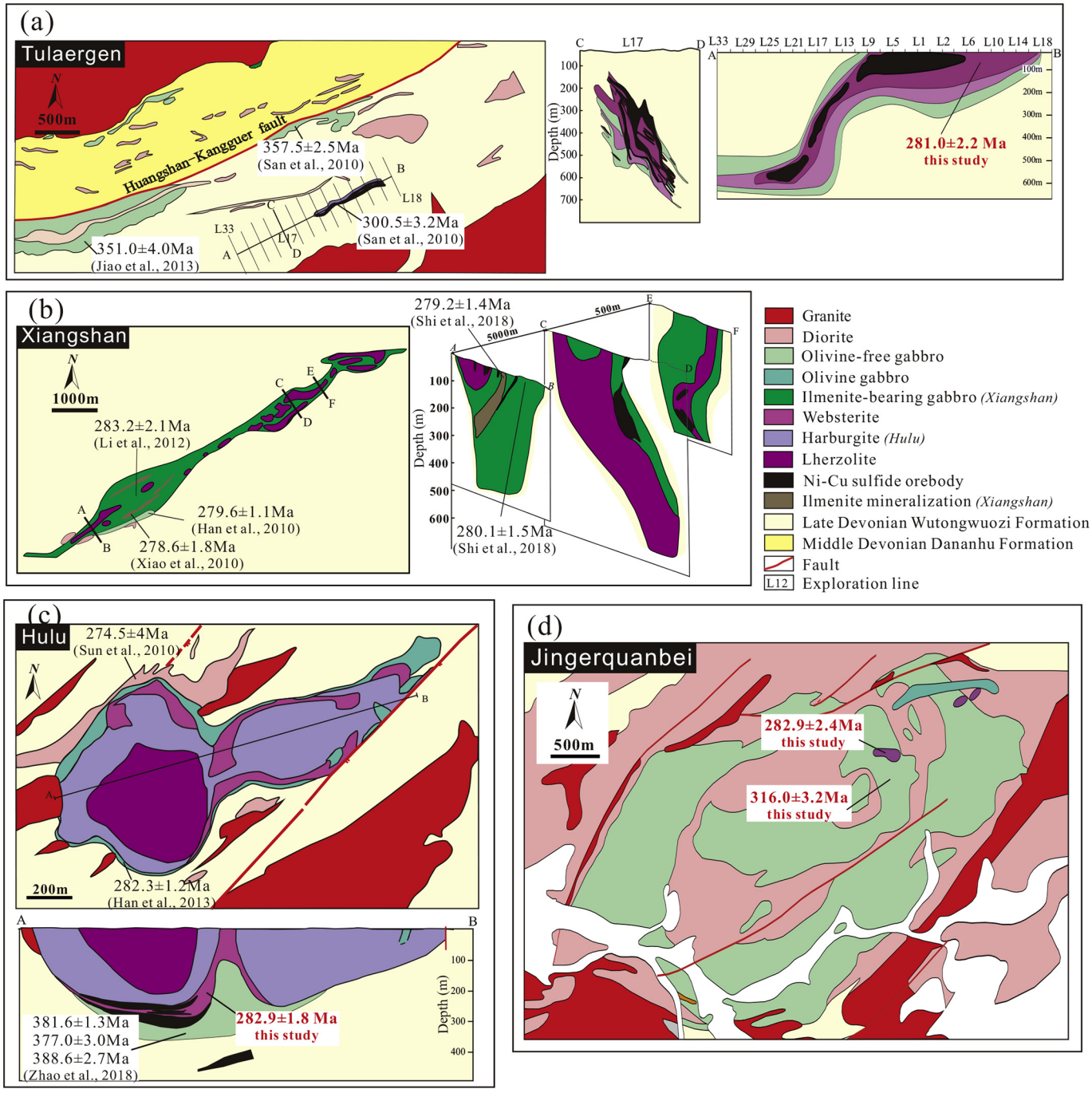

Fig. 3. The mafic-ultramafic complexes emplaced in the middle Devonian Wutongwuozi Formation after Zhao et al., 2018 and references therein. Simplified geological maps and selected cross sections show the dyke-like Ni-Cu sulfide-mineralized ultramafic bodies and relationships between the ultramafic facies and sulfide-barren olivine-free gabbro at Tulaergen (a), Xiangshan (b) and Jingerquanbei (d) as well as the elongate lopolith Hulu complexes (c). The olivine-free gabbros in the complexes are 300–380 Ma.

subduction (Han et al., 2013; Zhang et al., 2011), upwelling of asthenosphere due to break-off of subduction slab in syn- or post-collisional setting (Song et al., 2013) and the Tarim mantle plume (Pirajno et al., 2008; Qin et al., 2011). It is obviously not reasonable to simply regard the zircon U-Pb ages of the sulfide-barren gabbros as the time of the Ni-Cu sulfide mineralization due to the sharp contacts between the sulfide-mineralized and sulfide-barren facies. Thus, to convincingly constrain timings of the magmatism associated with the Ni-Cu sulfide mineralization, more geochronological measurements for the Ni-Cu sulfide-mineralized facies are necessary.

In this study, the zircons for U-Pb age dating are separated from 12 sulfide-mineralized ultramafic and mafic rocks and 3 sulfide-barren gabbros in 11 complexes. Integration of the new and previous age data offers a complete picture of the basaltic magmatism and Ni-Cu sulfide mineralization along the Huangshan-Jingerquan belt. The main objectives are to reveal the relationship between the Ni-Cu sulfide mineralization and the basaltic magmatism during development of the Huangshan-Jingerquan belt and to reconstruct the magma conduit system for the formation of the Ni-Cu deposits.

2. Geological background

The North Tianshan arc system, along the southern margin of the CAOB, between the Kelameili and Aqikkuduk faults, is divided by the Kanggur fault into the Harlik-Dananhu island arc in the north and the Kanggur-Yamansu arc in the south (Figs. 1a-c). The Kanggur-Yamansu arc is sub-divided into two parts by the Yamansu fault. The northern part is comprised of a middle Devonian (the Wutongwozi Formation) to late Carboniferous (the Gandun Formation) metasedimentary rock package and the southern part consists of Carboniferous volcanic and sedimentary sequences (Fig. 1d). Structural and paleomagnetic studies revealed that eastward movement of the Junggar block relative to Tarim blocks in ~300–240 Ma resulted in the dextral Main Tianshan Shear Zone (Figs. 1b and c, Laurent-Charvet et al., 2003; Wang et al., 2007). The Main Tianshan Shear Zone acted on the Kanggur-Yamansu arc and resulted in extensive deformation between the Kanggur and Yamansu faults (Fig. 1c, Branquet et al., 2012). Based on $^{40}Ar/^{39}Ar$ dating, Chen et al. (2005) proposed that the deformation initiated as early as ~300 Ma and extended to 250 Ma. The Huangshan-Jingerquan Ni-Cu metallogenic belt is located between the Kanggur and Yamansu faults (Figs. 2c and d).

3. Mafic-ultramafic complexes in the Huangshan-Jingerquan belt

The Huangshan-Jingerquan belt consists of a series of economic Ni-Cu sulfide deposits, such as Huangshan, Huangshandong, Tudun, Tulaergen, Hulu and Xiangshan (Table 1, Fig. 2D, Mao et al., 2008). The recent discovery of Ni-Cu sulfide mineralization in the Dahuangshan and Jingerquanbei complexes displays a great mineral exploration potential. The belt was divided into two parts by the Gandun fault (Fig. 1D). The northern part is occupied by the Wutongwozi Formation, which mainly consists of metasandstone with interlayers of tuff and marble (BGMRX, 1993). Our new LA-ICPMS data of detrital zircons from the metasandstones reveal a major U-Pb age population of 385–450 Ma (Deng et al., 2021). The youngest age (387 Ma) of the detrital zircons suggests that the maximum deposition age of the Wutongwozi Formation is middle Devonian. Accordingly, Devonian granitoid plutons (350–370 Ma, Zhou et al., 2010) were emplaced in the Wutongwozi Formation. The southern part is occupied by the Gandun Formation mainly consisting of siliceous slates and metasandstones with interlayers of marble (Fig. 1D, BGMRX, 1993). The youngest U-Pb age (307 Ma) of the detrital zircon age population of 491–301 Ma for the metasandstone (Deng et al., 2021) indicates that the Gandun Formation was deposited in late Carboniferous. This is consistent with ages of the granitoids emplaced in the formation (<290 Ma, Zhou et al., 2010).

It is remarkable that the mafic-ultramafic complexes emplaced in the Gandun and Wutongwozi formations have distinct lithology and geometry features. The mafic and ultramafic rocks in the complexes commonly contain 5–15 modal% hornblende and biotite, which are not in rock names in the text or in the figures to avoid long rock names.

3.1. The complexes emplaced in the late Carboniferous Gandun Formation

Relatively large mafic-ultramafic complexes are emplaced in the Gandun Formation (Table 1). Of them, the Huangshan and Huangshandong complexes host the largest Ni-Cu sulfide deposits, which contain 0.33 and 0.38 million tonnes Ni metal respectively, in the metallogenic belt.

The E-W trending Huangshan complex is ~2.5 km long and teardrop shaped with a shrinking tail to the east (Fig. 2A, Zhou et al., 2004). It is funnel-shaped in cross sections down to >1000 m at depths, which suggested magma feeder conduit in the west (Lightfoot and Evans-Lamswood, 2015). The main part of the complex comprises lherzolite and websterite, which gradually change to gabbronorite and olivine gabbro upward; the mineral modal variation indicates a magmatic differentiation sequence. However, a basal gabbronorite underlying the lherzolite and a small fine-grained lherzolite body overlying the gabbronorite at the surface with sharp contacts indicate intermittent emplacement of multiple pulses of magma (Fig. 2a, Deng et al., 2015, 2017 and references therein). Lenticular disseminated Ni-Cu sulfide ore bodies occur at the bases of the lherzolite and websterite and a few smaller ones are within the basal gabbronorite (Fig. 2a).

The ENE-WSW trending Huangshandong complex dominantly consisted of gabbroic rocks is 3.5 km long and up to 1.2 km wide with a perfect rhombic outline (Fig. 2b). Its undulating bottom extends to more than 1000 m deep in the western and middle portions and becomes shallow to the east. Lherzolite occurs as interlays within the ilmenite-bearing gabbro or between the ilmenite-bearing gabbro and olivine gabbro with sharp contacts (Fig. 2b). The olivine gabbro at the center of the complex is sharply contacted with the sulfide-barren olivine-free gabbro to the east, which is overlain by a lherzolite body at the eastern end of the complex. Diorite occurs along the complex margins. Such lithological relationships also show emplacement of multiple pulses of magma (Fig. 2b, Gao et al., 2013; Deng et al., 2014 and references therein). Disseminated Ni-Cu sulfide ore bodies are dominantly hosted by the lherzolite and a series of parallel concave lenticular ore bodies occur within the gabbronorite at western end of the complex (Fig. 2b).

The Huangshannan and Erhongwa complexes are similar to the Huangshandong complex in shape, size and rock assemblages, but with much smaller proportions of ultramafic rocks and weaker sulfide mineralization (Figs. 2c and d, Mao et al., 2017 and references therein). The small oval shape Tudun complex hosts stratiform Ni-Cu sulfide ore bodies within the lherzolite (Table 1, Fig. 2e, Wang et al., 2015).

3.2. The complexes emplaced in the middle Devonian Wutongwozi Formation

The complexes emplaced in the Wutongwozi Formation appear as a series of NE-SW trending dykes or pod chains (except for Hulu) (Fig. 3). The Xiangshan, Hulu and Tulaergen complexes hosted economic Ni-Cu sulfide deposits and the other very small complexes are weakly sulfide-mineralized (Table 1).

The Tulaergen complex consists of a mafic-ultramafic dyke and several stellate olivine-free gabbro intrusions devoid of sulfide. The ~800 m long mafic-ultramafic dyke hosts the third largest Ni-Cu sulfide deposit (~0.12 million tonnes Ni metal, Table 1) in the metallogeinc belt. The dyke steeply dips to southeast and becomes sub-horizontal tube-like tunnel toward to southwest at a depth of ~350 m within the metamorphosed clastic rocks (Fig. 3a). From the center to the margin, the rock type changes from lherzolite, through websterite, to olivine-free gabbro (San et al., 2010; Wang et al., 2018). Variably sized lenticular shaped Ni-Cu sulfide ore bodies are embedded in the lherzolite.

The Xiangshan complex is a NE-SW trending olivine gabbro dyke with a length of ~8 km and widths up to 1 km (Fig. 3b, Li et al., 1989 and references therein). Several lherzolite bodies containing disseminated Ni-Cu sulfides (up to 1 km long and 300 m wide) are enclosed within the olivine gabbro (Fig. 3b).

The Hulu complex is a ~2 km long and up to 1 km wide lopolith, which is shrunk in the middle (Table 1, Fig. 3c, Han et al., 2013). Lherzolite is underlain by harzburgite in the western portion of the lopolith and websterite occurs at the bottom. Stratiform Ni-Cu sulfide ore layers occur in the basal websterite. Sulfide-barren olivine-free gabbro occurs along the complex margins (Zhao et al., 2018).

The Jingerquanbei complex primarily comprises sulfide-barren olivine-free gabbro. A series of small sulfide-mineralized lherzolite bodies embed in the olivine-free gabbro on NE-SW direction (Fig. 3d). The other complexes emplace in the Wutongwozi Formation appear as NE-SW trending chains of small sparsely disseminated sulfide-mineralized ultramafic pods. For instance, the Mati complex is a

~1.6 km long chain consisting of a series of small ultramafic outcrops in the Gobi Desert (Table 1).

In summary, the complexes emplaced in both the Gandun and Wutongwozi formations share some common features, including: (1) Sharp contacts among the mafic and ultramafic facies cannot be attributed to magma differentiation but reflect intermittent emplacement of multiple pulses of magma (Figs. 2, 3); (2) Most of the Ni-Cu sulfide ore bodies are hosted in the ultramafic facies; (3) The olivine-free gabbro is sulfide-barren and the gabbros containing olivine may be sulfide-mineralized. However, the complexes emplaced in the Gandun Formation have large scales, teardrop, rhombic or oval outlines at the surface and funnel shaped vertical cross sections (Fig. 2, Lightfoot and Evans-Lamswood, 2015; Barnes et al., 2016), whereas, the ultramafic facies of the complexes emplaced in the Wutongwozi Formation are commonly steep dykes or chains of small pods, although the olivine-free gabbro may construct large intrusion (Fig. 3).

4. Sampling and analytical methods

Since zircon can crystalize from evolved basaltic magmas, mafic rock commonly contains more zircon than ultramafic rock (Grimes et al., 2005). Additionally, the sulfide ores can be more extensively altered than the sulfide-barren rocks. Thus, in previous U-Pb age dating of the Huangshan-Jingerquan complexes, the zircons were primarily separated from sulfide-barren gabbros, only 4 sulfide-mineralized rocks from the Huangshan and Huangshandong complexes were dated (Table 1). In this study, to constrain the timing of Ni-Cu sulfide mineralization along the Huangshan-Jingerquan belt, 12 sulfide-mineralized ultramafic and mafic rocks and 3 sulfide-barren rocks from eleven major complexes were chosen for zircon/baddeleyite separation. For the complexes without age data, such as the Jingerquanbei complexes, zircon/baddeleyite was separated from both sulfide-mineralized and sulfide-barren facies. The detailed information is summarized in Table S1.

4.1. Zircon separation

Separation of zircon and baddeleyite was completed by Nanjing Hongchuang Exploration Technology Service Co. Ltd.. The samples were crushed using a jaw crusher and disk mill to <250 μm and heavy minerals were then separated using an isodynamic magnetic separator and methylene iodide. Zircon and baddeleyite crystals were finally hand-picked under binocular microscope. Baddeleyite was separated from only five lherzolite and websterite samples (Table S1). The euhedral/subhedral prismatic and transparent zircon grains without obvious fractures or inclusions, 50 to 250 μm in diameter, are carefully mounted onto the epoxy together with the zircon standard TEMORA-2 (416.8 Ma, Black et al., 2004). Cathodoluminescence (CL) images (Appendix Fig. 1) were carried out on a Hitachi S3000N scanning electron microscope (SEM) at the Beijing SHRIMP Centre.

4.2. Zircon SHRIMP U-Pb dating

Eleven zircon samples were analyzed at Beijing SHRIMP Centre (National Science and Technology Infrastructure), China, using SHRIMP II following the analytical protocols of Compston et al. (1992) and Williams (1998) (Table S2a). Mass resolution of analytical sessions was ~5000 (1% definition). Spot size was 30 μm, and the intensity of the primary O^{2-} ion beam was 4 nA. Each spot was rastered for 150 s prior to analysis. Five scans through the mass stations were made for each age determination. Zircon standard M257 (561.3 Ma, U = 840 ppm, Nasdala et al., 2008) was measured to calibrate U, Th and Pb concentrations.

Three other zircon samples (HSX1, HSN1, MT18A) (Table S2a) were measured by using the SHRIMP II instrument at Australian National University (ANU), following the analytical protocols of Williams (1998). The intensity of the primary O^{2-} ion beam was 5 nA and spot sizes were 20 μm. Six scans through the mass stations were made for each age determination. Correction for common Pb was made according to the measured ^{204}Pb and the initial common lead composition for the likely age of the sample estimated using the two-stage terrestrial Pb evolution model of Stacey and Kramers (1975). U-Th abundance was calibrated based on the reference zircon SL13 (U = 238 ppm), which was in a separate set-up mount.

In both SHRIMP laboratories, zircon standard TEMORA-2 (416.8 Ma, Black et al., 2004) was used for isotopic fractionation correction. The ^{204}Pb-based method proposed by Stacey and Kramers (1975) was used for common Pb correction. The data were processed using SQUID 1.02/2.5 and Isoplot 3.0 programs of Ludwig (2001, 2003). Uncertainties for each analysis are expressed as 1σ. The weighted mean ages are quoted as 2σ.

4.3. Zircon LA-ICP-MS U–Pb dating

LA-ICP-MS analyses of two zircon samples (HSDD-01, HSDD-02) (Table S2b) were carried out on an Agilent 7900 Quadrupole ICP-MS coupled to a Photon Machines Analyte HE 193-nm ArF Excimer Laser Ablation system at Hefei University of Technology, China. Reference materials 91,500 zircon was used as external calibration for the U-Pb ages. Zircon GJ-1 or Plesovice were also analyzed between every 10 samples for quality control. Laser beam was 30 μm in diameter. The off-line data processing was performed using a program ICPMSDataCal (Liu et al., 2008). Time-dependent drifts of U-Th-Pb isotopic ratios were corrected using a linear interpolation (with time) for every five analyses according to the variations of 91,500 Wiedenbeck et al. (1995). Uncertainty of preferred values (±3 Ma) for the external standard Plesovic was propagated to the ultimate results of the samples. Concordia diagrams and weighted mean calculations were made using Isoplot 4.15 (Ludwig, 2011).

5. Results

The zircons from the sulfide-mineralized lherzolite, websterite and gabbros gave a narrow $^{206}Pb/^{238}U$ apparent age range of 289.4–271.0 Ma with concordant U/Pb ratios, showing no "high-U effect" (Tables S2a and S2b). These zircons yielded weighted mean $^{206}Pb/^{238}U$ ages ranging from 279.2 ± 2.6 to 284.2 ± 2.0 Ma with MSWD = 0.18–1.13 (SHRIMP) and = 1.3–2.3 (LA-ICPMS) (Table 1, Appendix Figs. 2 and 3). In contrast, the zircons from the olivine-free gabbros of the Jingerquanbei and Xianshuiquan complexes display much older $^{206}Pb/^{238}U$ apparent ages of >300 Ma with concordant U/Pb ratios within analytical uncertainties; the weighted mean $^{206}Pb/^{238}U$ ages of the zircons are 316.0 ± 3.2 Ma (MSWD = 0.74) and 380.4 ± 3.3 Ma (MSWD = 0.35), respectively (Table S2a, Fig. 5).

Our zircon U-Pb ages clearly illustrate that the sulfide-mineralized facies of the complexes emplaced in both the Gandun and Wutongwozi formations were formed from 279.2 ± 2.6 to 284.2 ± 2.0 Ma, within a very small interval of 280–285 Ma if analytical uncertainties are considered (Table 1, Appendix Figs. 2 and 3). For instance, the gabbronorite and lherzolite hosting Ni-Cu ore bodies in the Huangshan and Huangshandong complexes display zircon U-Pb age ranges of 280.5–284.5 Ma and 280.3–284.2 Ma, respectively. This is consistent with the previously published zircon U-Pb ages of the gabbronorite (283.8 ± 3.4 Ma and 284.5 ± 2.5 Ma by Qin et al., 2011 and Gu et al., 2006) from the Huangshan complex and the lherzolite and olivine gabbro (281.4 ± 2.2 Ma and 280.3 ± 1.9 Ma by Mao et al., 2019) from the Huangshandong complex (Table 1. Figs. 2a, b). In contrast, previous and our new zircon U-Pb age data indicate that the sulfide-barren olivine-free gabbro and diorite have ages ranging from 380 Ma to 267 Ma (Table 1, Fig. 4).

The zircons from the sulfide-mineralized mafic/ultramafic rocks have large variations in U and Th (40–5592 ppm and 35–24,103 ppm, respectively, and Th/U ratios of 0.2–9.7) (Appendix Fig. 4). Uranium and Th are commonly higher in continental crust than in basalts and

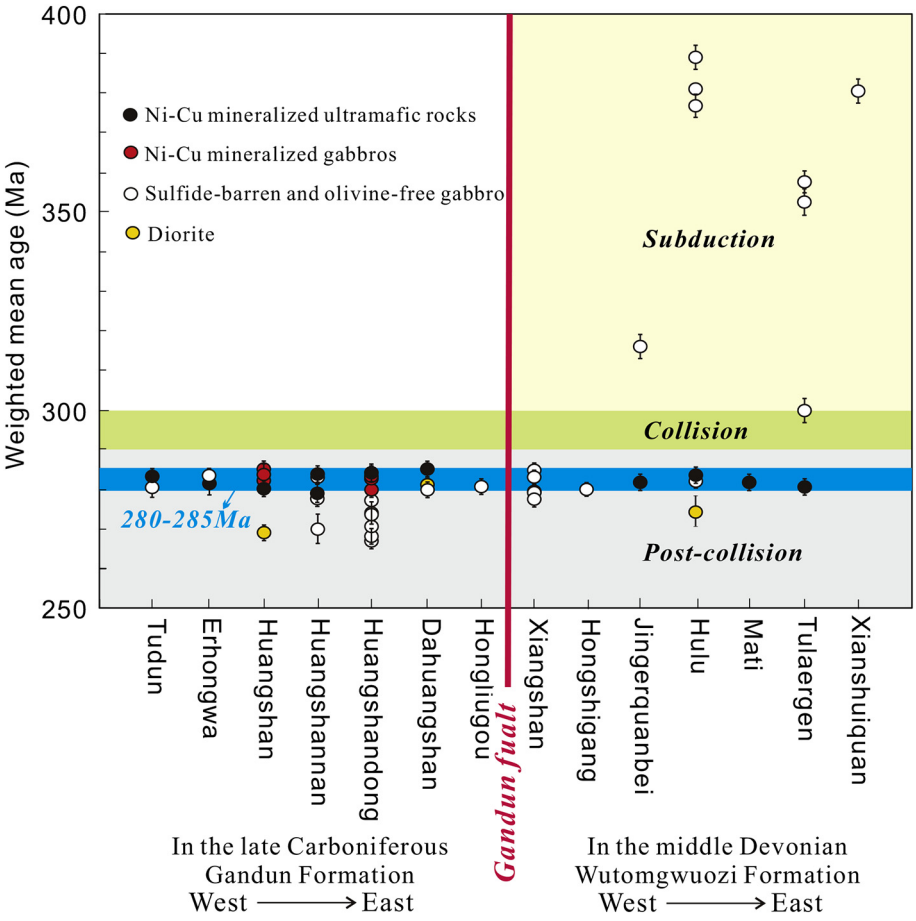

Fig. 4. Integration of zircon U-Pb ages of the mafic and ultramafic facies in the complexes of the Huangshan-Jingerquan belt. The sulfide-mineralized mafic and ultramafic rocks have dates between 280 and 285 Ma taking into account measurement error. The olivine-free gabbros older than 300 Ma are sulfide-barren and only occur in the complexes emplaced in the middle Devonian Wutongwozi Formation. The gabbro and diorite younger than 280 Ma are sulfide barren. The age data are listed in Table 1 and the age data of the Dahuangshan complex are unpublished.

incompatible for mafic minerals and compatible for zircon (Grimes et al., 2007). As one of the lastest crystalized minerals in mafic and ultramafic rocks, zircon can enrich in U and Th. Thus, the large variations of U and Th in the zircons from the sulfide-mineralized rocks were most likely resulted from magmatic differentiation and crustal contamination (Appendix Fig. 4). Whereas, relatively weak differentiation and crustal contamination resulted in the zircons from the sulfide-barren olivine-free gabbros having low U (26–968 ppm) and Th (8–1024 ppm) with Th/U ratios of 0.3–1.2.

6. Discussion

The sulfide-mineralized and sulfide-barren facies of some complexes from the Huangshan-Jingerquan belt have different ages (Table 1), rather than a single age group. For instance, although the gabbroic facies and lherzolite in the western portion of the Huangshandong complex have similar zircon U-Pb ages of 280.3 ± 1.9 Ma to 284.2 ± 2.0 Ma, the olivine-free gabbro, which is sharply contacted with the olivine gabbro and occupies the eastern portion of the complex, yield younger ages, ranging from 277.0 ± 1.1 Ma to 267.0 ± 2.1 Ma (Fig. 2b). Although most of the zircon U-Pb ages for the olivine-free gabbro were measured using LA-ICPMS method, they are well consistent with the zircon SHRIMP U-Pb age (274.0 ± 3.0 Ma) (Table 1). This is consistent with the sharp contact between the two facies (Fig. 2b). Thus, it is convincible that the olivine-free gabbro is younger than the olivine gabbro. The websterite and marginal olivine gabbro of the Hulu complex exhibited similar zircon U-Pb ages (282.9 ± 1.8 Ma and 282.3 ± 1.2 Ma, respectively), whereas the basal olivine-free gabbros show U-Pb ages of 377.0 ± 3.0 to 388.6 ± 2.7 Ma, and the diorite displays an age of 274.5 ± 4 Ma (Fig. 3c, Table 1). Some questions are needed to be addressed: (1) Were the complexes emplaced in the Gandun and Wutongwozi formations result from disparate basaltic magmatisms in different tectonic periods? (2) If the sulfide-mineralized mafic and ultramafic facies and sulfide-barren gabbros did take place in different periods? (3) Why are the complexes emplaced in the Ganduan and Wutongwozi formations diverse in geometry? The most important issue is to examine the new and previous zircon U-Pb age data based on relationship between periods of the basaltic magmatism and tectonic evolution of the North Tianshan arc system.

6.1. Implications of the Zircon U-Pb ages

The complexes containing 300–380 Ma olivine-free gabbros are only emplaced in the Wutongwozi Formation and those having olivine-free gabbro and diorite younger than 280 Ma are emplaced in both the Wutongwozi and Gandun formations (Table 1, Appendix Figs. 2 and 3). Correspondingly, the 350–370 Ma granitoid plutons are emplaced in the Wutongwozi Formation, whereas those younger than 300 Ma may be embedded in both the Wutongwozi and Gandun formations (Fig. 1d, Zhou et al., 2010; Han and Zhao, 2018). This is consistent with the deposition times of the Wutongwozi and Gandun formations. Thus, the prolonged basaltic magmatism along the Huangshan-Jingerquan belt can be divided into three periods. The first period magmatism resulted in the 300–380 Ma sulfide-barren olivine-free

gabbros; the second period magmatism produced the 280–285 Ma sulfide-mineralized mafic and ultramafic rocks; the third period magmatism generated the sulfide-barren olivine-free gabbro and diorite younger than 280 Ma (Fig. 4). This means that the basaltic magmatism associated with the Ni-Cu sulfide mineralization was short-lived (~280–285 Ma), although the basaltic magmatism along the Huangshan-Jingerquan belt are prolonged (380–265 Ma).

It is important to point out that ages of the sulfide-mineralized facies of the complexes (~280–285 Ma) are coincident with the peak of magmatism in the Tarim Basin (~290–280 Ma). This implies a possible contribution of the Tarim mantle plume to the formation of the mafic-ultramafic complexes in the Eastern Tianshan and Beishan regions (Qin et al., 2011). However, compositions of trace elements and Sr-Nd isotopes of the mafic-ultramafic complexes in the Eastern Tianshan and Beishan regions are distinct from those in the Tarim Basin (Song et al., 2013; Xue et al., 2016). Additionally, the Permian Tarim mantle plume could not account for the 300–380 Ma gabbros in the Huangshan-Jingerquan complexes. Thus, the prolonged basaltic magmatism along the Huangshan-Jingerquan belt was more likely associated with subduction-collision processes. An alternative view is that the Permian mafic-ultramafic rocks in the Eastern Tianshan and Beishan regions are the products of basaltic magmatism induced by lithospheric delamination and asthenosphere upwelling in a convergent zone (Xue et al., 2016).

Recent geochronology and geochemistry studies demonstrated that the Carboniferous calc-alkaline volcanics in the Kanggur-Yamansu arc were resulted from subduction of the North Tianshan Ocean (e.g., Chen et al., 2013; Wang et al., 2014; Xiao et al., 2015). The occurrences of the 305–290 Ma Permian bimodal volcanics within the Harlik-Dananhu arc and the 250–290 Ma A_2-type granitoids in the Kanggur-Yamansu arc were attributed to post-collisional magmatism (Han and Zhao, 2018; Shu et al., 2011). Thus, collisions among the arcs in the North Tianshan Ocean most likely occurred in latest Carboniferous to early Permian (Han and Zhao, 2018; Xiao et al., 2019). These studies indicated that the North Tianshan arc system experienced three tectonic periods: (1) two-way subduction of the North Tianshan Ocean in Ordovician-Carboniferous (before ~300 Ma), (2) collision between the Harlik-Dananhu and Kanggur-Yamansu arcs in the latest Carboniferous to early Permian (~300–290 Ma) and (3) post-collision tectonics in Permian (after ~290 Ma). Chen et al. (2019) recognized that the 300–480 Ma detrital zircons from the Carboniferous clastic rocks in both the Kanggur-Yamansu arc and the Central Tianshan block have similar $E_{Hf(t)}$ values. The accretionary prism and volcanic zone of the Kanggur-Yamansu arc were developed at the northern margin of the Central Tianshan block and the North Tianshan Ocean was most likely terminated along the Kanggur fault (Fig. 1d) (Chen et al., 2019; Xiao et al., 2019).

Therefore, we propose that the sulfide-barren olivine-free gabbros prior to 285 Ma and after 280 Ma along the Huangshan-Jingerquan belt were formed in subduction and post-collision periods, respectively (Fig. 4). Absence of olivine in these gabbros suggests low degree partial melting of the upper mantle. In contrast, the 280–285 Ma mafic/ultramafic rocks are corresponding to a relatively high degree partial melting event. This is supported by the up to 86–89 forsterite percentages of the olivine in the sulfide-mineralized ultramafic rocks, which demonstrate the emplacement of high-Mg basaltic magmas (Deng et al., 2017; Zhou et al., 2004). Compositions of clinopyroxene from the ultramafic rocks and positive correlation between TiO_2 and $(Fe_2O_3)_T$/MgO in whole-rocks of the Huangshan-Jingerquan complexes revealed a tholeiitic affinity (Song et al., 2013). Whole-rock trace element and lead isotope compositions as well as major oxide compositions of the chromite from the ultramafic rocks demonstrated contributions from both asthenosphere and mantle wedge (Song et al., 2013). Thus, the high-Mg tholeiitic magma along the Huangshan-Jinerquan belt was most likely generated by the short-lived melting of the hydrated hot asthenosphere inflow into the slab window in early post-collisional period following onset of the collision between the Harlik-Dananhu arc and the Kanggur-Yamansu arc (Fig. 4).

The short-lived high-Mg tholeiitic magmatism associated with slab break-off in collision zone is supported by numerical modeling (Duretz et al., 2011; Freeburn et al., 2017; Van Hunen and Allen, 2011). The denser oceanic lithosphere will be inevitably detached from the more buoyant continental lithosphere after the onset of continental collision (Davies and von Blanckenburg, 1995; Duretz et al., 2011). Slab break-off occurs, often taking tens of millions of years after initial collision, in depths of 40 to >500 km depending on strength of the oceanic plate and extends laterally very fast (Ferrari, 2004; Van Hunen and Allen, 2011). Under most circumstances, slab break-off occurs at depths too large to induce decompression melting of dry upwelling asthenosphere (Davies and von Blanckenburg, 1995). However, water released from the tip of the detached slab may prompt hydration and extensive melting of the rising asthenosphere within a few million years (Freeburn et al., 2017).

It is noteworthy that a few of sulfide-mineralized mafic-ultramafic intrusions were formed during a subduction period along the southern margin of the CAOB, such as the Heishan intrusion (~357 Ma, Xie et al., 2012) (Fig. 1c). Recent studies regarded generation of the related basaltic magmas as partial melting of upwelling asthenosphere due to accidental slab break-off during subduction (Xie et al., 2014; Yang and Zhou, 2009). However, these deposits are much smaller than those along the Huangshan-Jingerquan belt. Thus, the most important period for the formation of Ni-Cu sulfide deposit in orogenic belt is the early post-collision period.

6.2. Roles of regional strike-slip shearing

Recent studies indicated that the regional strike-slip shearing along the Huangshan-Jingerquan belt began at ~300 Ma simultaneously with the collision between the Harlik-Dananhu and Kanggur-Yamansu arcs (~300–290 Ma) (Chen et al., 2005 and references therein). This permits us to speculate that the collision overlapping with the regional shearing accelerated the slab break-off and upwelling of hot asthenosphere. This process intensified relatively high degree melting of the hydrated asthenosphere and generation of the voluminous high-Mg tholeiitic magma, which is critical for the formation of the mafic and ultramafic facies in the complexes along the Huangshan-Jingerquan belt in 280–285 Ma.

Based on petro-structural analysis and strain rate calculation, Branquet et al. (2012) proposed that regional strike-slip shearing created transtensive spaces for ascending of the basaltic magma and formation of magma chambers. Thus, the Huangshan and Huangshandong complexes have teardrop and rhombic shapes and the wall rocks have been tightly folded with long axis parallel to the foliation (Fig. 2b, Lightfoot and Evans-Lamswood, 2015). Therefore, coupling of the regional shearing with collision is very important for generation and emplacement of the high-Mg tholeiitic magmas and the Ni-Cu sulfide mineralization in 280–285 Ma (Fig. 4).

6.3. Implications of geometry of the complexes

Although it is difficult to figure out when attitudes of the stratum were deformed, it is clear that the late Carboniferous Gandun Formation was originally above the middle Devonian Wutongwozi Formation. Therefore, we speculate that the steep sulfide-mineralized ultramafic dykes and pod chains in the Wutongwozi Formation are most likely the residues of sub-vertical magma pathways at deep levels (Fig. 3). Whereas the large rhombic, teardrop or oval shaped complexes emplaced in the Gandun Formation represent the shallow magma chambers along magma conduit systems (Fig. 2). The sulfide liquids were carried by ascending basaltic magmas and deposited in different depths along the magma conduit system to form the sulfide-mineralized dykes and complexes. Similar magma conduit system was

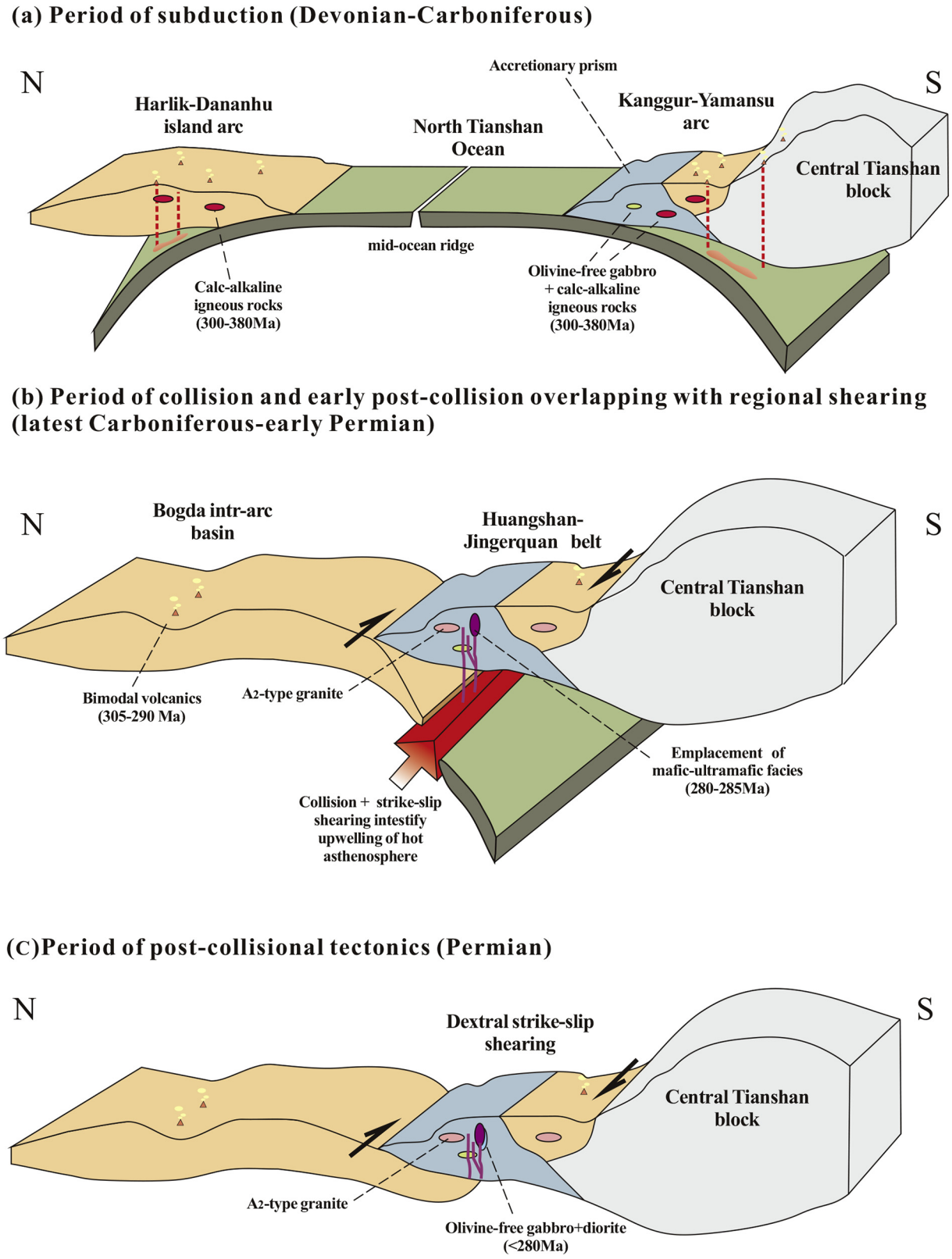

Fig. 5. Schematic diagrams illustrating the tectonic-magmatism in the North Tianshan arc system. (a) Two-way subduction of the North Tianshan Ocean created the Harlik-Dananhu island arc and the Kanggur-Yamansu arc at the northern margin of the Central Tianshan block and resulted in >300 Ma sulfide-barren olivine-free gabbro. (b) Coeval collision and strike-slip shearing intestified slab break-off and upwelling of asthenosphere and the 280–285 Ma high-Mg basaltic magmatism and Ni-Cu mineralization along the Huangshan-Jingerquan belt. (c) Post-collisional magmatism resulted in sulfide-barren gabbro and diorite.

recognized at Voisey's Bay, Canada, where disseminated sulfides-bearing dykes or veins occur in deep levels and the intrusions containing large sulfide ore bodies occur in shallow depths (e.g. Lightfoot et al., 2012; Ripley and Li, 2011). Alternatively, it cannot be completely rule out that the distinct outlines of the complexes emplaced in the two strata merely reflect the geometry features of the complexes, because relative depths of the two strata might have been changed by early Permian tectonic movement.

6.4. Model of basaltic magmatism and Ni-Cu mineralization in the Huangshan-Jingerquan belt

The prolonged basaltic magmatism and short-lived magmatic Ni-Cu sulfide mineralization along the Huangshan-Jingerquan belt recorded by the zircon U-Pb age data (Table 1, Fig. 4) are closely related to three tectonic periods of the North Tianshan arc system.

6.4.1. Period of subduction (Fig. 5a)

Two-way subduction of the North Tianshan Ocean not only produced the Paleozoic calc-alkaline volcanics in the Harlik-Dananhu island arc to the north and the Kanggur-Yamansu arc to the south, but also the 300–380 Ma gabbros and granites emplaced in the Wutongwozi Formation along the Huangshan-Jingerquan belt. The gabbros are olivine-free and sulfide-barren due to low degree partial melting.

6.4.2. Period of collision to early post-collision overlapping with regional shearing (Fig. 5b)

Collision between the Harlik-Dananhu and the Kanggur-Yamansu arcs at the latest Carboniferous (~300–290 Ma) was overlapped with regional strike-slip shearing. Such process intensified slab break-off and hot asthenosphere upwelling through the "slab window" tens of millions years after the onset of collision. Introduction of water released from the detached slab induced extensive melting of the upwelling asthenosphere and generated voluminous high-Mg tholeiitic magmas between 280 and 285 Ma. The basaltic magmatism was short-lived as the asthenospheric melting will die down when the water released from the slab was exhausted (Freeburn et al., 2017). The transcrustal fractures produced by the regional shearing provided pathways for ascending basaltic magmas. In such magma plumbing system, sulfide liquid immiscibility occurred in deep levels and the sulfides were captured and carried by ascending basaltic magma. During migration upward, a limited amount of the sulfides was deposited at locations where the magma pathways were broadened or turned off and formed the sulfide-mineralized ultramafic dykes or chains of pods in the Wutongwozi Formation (Fig. 3). The sulfide-bearing ultramafic pods might be embedded into the early formed bodies of sulfide-barren olivine-free gabbros, such as in the Jingerquanbei complex, due to reactivation of pre-existing structures. More sulfide liquids were further carried upward to large magma chambers at shallower depths and cumulated to form large ore bodies, such as in the Huangshan and Huangshandong complexes emplaced in the Gandun Formation (Fig. 2).

6.4.3. Period of post-collisional tectonics (Fig. 5c)

Magmatisim in post-collisional extension event produced the sulfide-barren olivine-free gabbro and diorite younger than 280 Ma, which commonly intruded into the complexes using the same transcrustal fractures along the Huangshan-Jingerquan belt (Table 1, Fig. 4). As the water released from the detached slab was exhausted and the slab rapidly sinks downward, the degrees of partial melting decrease significantly (Freeburn et al., 2017). As a result, the sulfide-barren gabbro and diorite are absent of olivine.

7. Conclusions

The prolonged basaltic magmatism along the Huangshan-Jingerquan metallogenic belt is closely related to tectonic evolution of the North Tianshan arc system. Subduction-related basaltic magmatism produced the 300–380 Ma sulfide-barren olivine-free gabbros. Following the closure of the North Tianshan Ocean in ~300–290 Ma, collision combined with regional strike-slip shearing led to slab break-off and upwelling of hot asthenosphere in early post-collision period. Releasing of water from the broken slab induced extensive melting of the upwelling asthenosphere and generated voluminous high-Mg tholeiitic magma in 280–285 Ma. The regional shearing created fracture networks as pathways for the ascending basaltic magma and transtensive spaces for the magma chambers at different depths. In such a magma plumbing system, deposition of the sulfides carried by the basaltic magma along the pathways formed the sulfide-mineralized ultramafic dykes in deep levels; more sulfides were carried to shallow magma chambers and cumulated along with mafic minerals forming the Ni-Cu sulfide orebodies, sulfide-mineralized mafic and ultramafic facies in the complexes. The sulfide-barren olivine-free gabbros and diorites younger than 280 Ma are the products of low-degree partial melting of the relatively dry upper mantle in post-collisional extension environment. Thus, we propose that early post-collision concurrent with regional strike-slip shearing is the optimal condition for the formation of economic Ni-Cu sulfide deposit in orogenic belt.

Declaration of Competing Interest

The authors declare that they have no known competing financial interests or personal relationships that could have appeared to influence the work reported in this paper.

Acknowledgement

The authors would like to thank Mr. Gang Deng, Jun-Hui Xie, Wei-Dong Li and graduate students Kai-Yuan Wang, Jian Kang, Jin-Jin Zhu, and Shuai Wei for their assistance with field work. Fruitful discussions with Dr. Steve Barnes and Prof. Ke-Zhang Qin is greatly acknowledged and appreciated. Thanks are due to Dr. Hang-Qiang Xie and Fang-Yao Wang for SHRIMP analysis. We would like to express gratitude to Prof. Xian-Hua Li and Chusi Li and the anonymous reviewer for their helpful comments and suggestions. This study was financially supported by funds from National Key Research and Development Program of China (2018YFA0702605) and the NSFC research grants (41630316, 41772067, 41873031 and U1803113).

Appendix A. Supplementary data

Supplementary data to this article can be found online at https://doi.org/10.1016/j.lithos.2021.106114.

References

Barnes, S.J., Makkonen, H.V., Dowling, S.E., Hill, R.E.T., Peltonen, P., 2009. The 1.88 Ga Kotalahti and Vammala Nickel Belts, Finland: geochemistry of the mafic and ultramafic metavolcanic rocks. Bull. Geol. Soc. Finl. 81, 103–141.

Barnes, S.J., Cruden, A.R., Arndt, N., Saumur, B.M., 2016. The mineral system approach applied to magmatic Ni-Cu-PGE sulphide deposits. Ore Geol. Rev. 76, 296–316.

BGMRX, 1993. Regional Geology of Xinjiang Uygur Autonomous Region, Bureau of Geology and Mineral Resources of Xinjiang Uygur Autonomous Region Geological Memoirs. Geological Publishing House Beijing (in Chinese).

Black, L.P., Kamo, S.L., Allen, C.M., Davis, D.W., Aleinikoff, J.N., Valley, J.W., Mundil, R., Campbell, I.H., Korsch, R.J., Williams, I.S., Foudoulis, C., 2004. Improved $^{206}Pb/^{238}U$ microprobe geochronology by the monitoring of a trace-element-related matrix effect; SHRIMP, ID-TIMS, ELA-ICP-MS and oxygen isotope documentation for a series of zircon standards. Chem. Geol. 205, 115–140.

Branquet, Y., Gumiaux, C., Sizaret, S., Barbanson, L., Wang, B., Cluzel, D., Li, G., Delaunay, A., 2012. Synkinematic mafic/ultramafic sheeted intrusions: emplacement mechanismand

strain restoration of the Permian Huangshan Ni–Cu ore belt (Eastern Tianshan, NW China). J. Asia Earth Sci. 56, 240–257.
Chen, W., Sun, S., Zhang, Y., Xiao, W.-J., Wang, Y.-T., Wang, Q.-L., Jiang, L.-F., Yang, J.-T., 2005. $^{40}Ar/^{39}Ar$ geochronology of the Qiugemingtashi-Huangshan ducile shear zone in East Tianshan, Xinjiang, NW China. Acta Geol. Sin. 79 (6), 790–804 (in Chinese with English abstract).
Chen, X.J., Shu, L.S., Santosh, M., Zhao, X.X., 2013. Island arc-type bimodal magmatism in the eastern Tianshan Belt, Northwest China: geochemistry, zircon U-Pb geochronology and implications for the Paleozoic crustal evolution in Central Asia. Lithos 168, 48–66.
Chen, Z., Xiao, W.-J., Windley, B.F., Schulmann, K., Mao, Q., Zhang, Z., Zhang, J., Deng, C., Song, S., 2019. Composition, provenance and tectonic setting of the Southern Kangurtag accretionary complex in the Eastern Tianshan, NW China: implications for the late Paleozoic evolution of the North Tianshan Ocean. Tectonics 38, 2779–2802.
Compston, W., Williams, I.S., Kirschvink, J.L., 1992. Zircon U-Pb ages for the early Cambrian timescale. J. Geol. Soc. Lond. 149, 171–184.
Davies, J.H., von Blanckenburg, F., 1995. Slab break-off: A model of lithospheric detachment and its test in the magmatism and deformation of collisional orogens. Earth Planet. Sci. Lett. 129, 85–102.
Deng, Y.-F., Song, X.-Y., Chen, L.-M., Zhou, T.-F., Pirajno, F., Yuan, F., Xie, W., Zhang, D.-Y., 2014. Geochemistry of the Huangshandong Ni-Cu deposit in northwestern China: implications for the formation of magmatic sulfide mineralization in orogenic belts. Ore Geol. Rev. 56, 181–198.
Deng, Y.-F., Song, X.-Y., Hollings, P., Zhou, T., Yuan, F., Chen, L.-M., Zhang, D.-Y., 2015. Role of asthenosphere and lithosphere in the genesis of the Early Permian Huangshan mafic-ultramafic intrusion in the Northern Tianshan, NW China. Lithos 227, 241–254.
Deng, Y.-F., Song, X.-Y., Hollings, P., Chen, L.-M., Zhou, T., Yuan, F., Xie, W., Zhang, D., Zhao, B., 2017. Lithological and geochemical constraints on the magma conduit systems of the Huangshan Ni-Cu sulfide deposit, NW China. Mineral. Deposita 52, 845–862.
Deng, Y.-F., Yuan, F., Hollings, P., Song, X.-Y., Zhou, T., Fu, B., Denyszyn, S., Zhao, B., 2020. Magma generation and sulfide saturation of Permian mafic-ultramafic intrusions from the western part of the Northern Tianshan in NW China: implications for Ni-Cu mineralization. Mineral. Deposita 55, 515–534.
Deng, Y.-F., Song, X.-Y., Jie, W., Yuan, F., Zhao, Z.-M., Wei, S., Zhu, J.-J., Kang, J., Wang, K.-Y., Liang, Q.-L., Chen, L.-M., Yu, S.-Y., 2021. Determination of sedimentary ages of the strata in the Huangshan-Jingerquan metallogenic belt and its geological significances. Acta Geol. Sin. 95 (2), 362–376 (in Chinese with English abstract).
Duretz, T., Gerya, T.V., May, D.A., 2011. Numerical modelling of spontaneous slab breakoff and subsequent topographic response. Tectonophysics 502, 244–256.
Ferrari, L., 2004. Slab detachment control on mafic volcanic pulse and mantle heterogeneity in central Mexico. Geology 32 (1), 77–80.
Freeburn, R., Bouilhol, P., Maunder, B., Magni, V., ven Hunen, J., 2017. Numerical models of the magmatic processes induced by slab breakoff. Earth Planet. Sci. Lett. 478, 203–213.
Gao, J.-F., Zhou, M.-F., Lightfoot, P.C., Wang, C.Y., Qi, L., Sun, M., 2013. Sulfide saturation and magma emplacement in the formation of the Permian Huangshandong Ni-Cu sulfide deposit, Xinjiang, Northwestern China. Econ. Geol. 108, 1833–1848.
Godel, B., Seat, Z., Maier, W.D., Barnes, S.-J., 2011. The Nebo-Babel Ni-Cu-PGE sulfide deposit (West Musgrave Block, Australia): Pt. 2. Constraints on parental magma and processes, with implications for mineral exploration. Econ. Geol. 106, 577–584.
Grimes, C.B., John, B.E., Cheadle, M.J., Schwartz, J.J., Mazdab, F.K., Wooden, J.L., Reiners, P.W., 2005. Widespread occurrence of zircon in slow and ultra-slow spreading ocean crust: a tool for studying oceanic lithospheric processes. Eos 86, 1535.
Grimes, C.B., John, B.E., Kelemen, P.B., Mazdab, F.K., Wooden, J.L., Cheadle, M.J., Hanghoj, K., Schwaetz, J.J., 2007. Trace element chemistry of zircons from oceanic crust: a method for distinguishing detrital zircon provenance. Geology 35, 643–646.
Gu, L.X., Zhang, Z.Z., Wu, C.Z., Wang, Y.X., Tang, J.H., Wang, C.S., Xi, A.H., Zheng, Y.C., 2006. Some problems on granites and vertical growth of the continental crust in the eastern Tianshan Mountains, NW China. Acta Petrol. Sin. 22, 1103–1120 (in Chinese with English abstract).
Han, Y., Zhao, G., 2018. Final amalgamation of the Tianshan and Junggar orogenic collage in the southwestern Central Asian Orogenic Belt: constraints on the closure of the Palo-Asian Ocean. Earth Sci. Rev. 186, 129–152.
Han, B.F., Ji, J.Q., Song, B., Chen, L.H., Li, Z.H., 2004. SHRIMP U-Pb zircon age of the mafic-ultramafic rocks and geological significance in Karatungk and Huangshan. Xinjiang: Chinese Sci. Bullet. 49, 2324–2328 (in Chinese with English abstract).
Han, C.-M., Xiao, W.-J., Zhao, G.-C., Su, B.-X., Saky, P.A., Ao, S.-J., Wan, B., Zhang, J., Zhang, Z.-Y., 2013. SIMS U-Pb zircon dating and Re-Os isotopic analysis of the Hulu Cu-Ni deposit, eastern Tianshan, Central Asian Orogenic Belt, and its geological significance. J. Geol. 58, 251–270.
Jiao, J.G., Zhang, P.P., Liu, R.P., Duan, J., Jiang, C., 2013. SHRIMP zircon U-Pb age of the No. 3 intrusion in the Tulaergen Cu-Ni mining area, East Tianshan Muntain, Xinjiang and its geological significance. Geol. Explor. 49 (3), 393–404 (in Chinese with English abstract).
Laurent-Charvet, S., Charvet, J., Monie, P., Shu, L.S., 2003. Late Paleozoic strike-slip shear zones in eastern Central Asia (NW China): new structural and geochronological data. Tectonics 22, 1099–1101.
Li, D.-H., Bao, X.-C., Zhang, B.-N., Han, Z.-W., Zhu, G.-Q., Zeng, Z.-X., 1989. Investigation of geology, geophysics and geochemistry of the Huangshan Cu–Ni metallogenic belt for mineral exploration. Report of the National 305 Project of China (in Chinese).
Li, D.D., Wang, Y.W., Wang, J.B., Wang, L.J., Long, L.L., Liao, Z., 2012. The timing order of mineralization and diagenesis for Xiangshan complex rocks, Xinjiang. Acta Petrol. Sin. 28, 2103–2112 (in Chinese with English abstract).
Li, C., Zhang, Z., Li, W., Wang, Y., Sun, T., Ripley, E.M., 2015. Geochronology, petrology and Hf-S isotope geochemistry of the newly discovered Xiarihamu magmatic Ni-Cu sulfide deposit in the Qinghai-Tibet plateau, western China. Lithos 216-217, 224–240.
Li, C., Ripley, E.M., Tao, Y., 2019. Magmatic Ni-Cu and Pt-Pd sulfide deposits in China. Soc. Econ. Geol. Spec. Publ. 22, 483–508.
Lightfoot, P.C., Evans-Lamswood, D., 2015. Structural controls on the primary distribution of mafic-ultramafic intrusions containing Ni-Cu-Co-(PGE) sulfide mineralization in the roots of large igneous provinces. Ore Geol. Rev. 64, 354–386.
Lightfoot, P.C., Keays, R.R., Evans-Lamswood, D.E., Wheeler, R., 2012. S saturation history of Nain Plutonic Suite mafic intrusions: origin of the Voisey's Bay Ni-Cu-Co sulfide deposit, Labrador, Canada. Mineral. Deposita 47, 23–50.
Liu, Y., Hu, Z., Gao, S., Günther, D., Xu, J., Gao, C., Chen, H., 2008. In situ analysis of major and trace elements of anhydrous minerals by LA-ICP-MS without applying an internal standard. Chem. Geol. 257, 34–43.
Liu, Y.G., Li, W.Y., Jia, Q.Z., Zhang, Z.W., Wang, Z.A., Zhang, Z.B., Zhang, J.W., Qian, B., 2018. The dynamic sulfide saturation process and a possible slab break-off model for the giant Xiarihamu magmatic nickel ore deposit in the East Kunlun Orogenic Belt, Northern Qinghai-Tibet Plateau, China. Econ. Geol. 113, 1383–1417.
Ludwig, K.R., 2001. SQUID 1.02, A User's Manual, Berkeley Geochronology Center Special Publication No.2. p. 17.
Ludwig, K.R., 2003. Isoplot 3.0: A Geochronological Toolkit for Microsoft Excel. Berkeley Geochronology Centre, Spec. Publ. 4 pp. 1–70.
Ludwig, K.R., 2011. Isoplot v. 4.15: A geochronological toolkit for Microsoft Excel. Berkeley Geochronology Center Special Publication 4. p. 75.
Maier, W.D., Barnes, S.-J., Chinyepi, G., Barton Jr., J.M., Eglington, B., Setshedi, I., 2008. The composition of magmatic Ni-Cu-(PGE) sulfide deposits in the Tati and Selebi-Phikwe belts of eastern Botswana. Mineral. Deposita 43, 37–60.
Maier, W.D., Smithies, R.H., Spaggiari, C.V., Barnes, S.J., Kirkland, C.L., Yang, S., Lahaye, Y., Kiddie, O., MacRae, C., 2016. Petrogenesis and Ni-Cu sulphide potential of mafic-ultramafic rocks in the Mesoproterozoic Fraser Zone within the Albany-Fraser Orogen, Western Australia. Precambrian Res. 281, 27–46.
Mao, J.W., Pirajno, F., Zhang, Z.H., Chai, F.M., Wu, H., Chen, S.P., Zhang, C.Q., 2008. A review of the Cu-Ni sulphide deposits in the Chinese Tianshan and Altay orogens (Xinjiang Autonomous Region, NW China): principal characteristics and ore-forming processes. J. Asian Earth Sci. 32, 184–203.
Mao, Y.J., Qin, K.Z., Tang, D.M., Feng, H.Y., Xue, S.C., 2016. Crustal contamination and sulfide immiscibility history of the Permian Huangshannan magmatic Ni-Cu sulfifide deposit, East Tianshan, NW China. J. Asia Earth Sci. 129, 22–37.
Mao, Y.J., Qin, K.Z., Barnes, S.J., Tang, D.M., Xue, S.C., Vaillant, M.L., 2017. Genesis of the Huangshannan high-Ni tenor magmatic sulfifide deposit in the Eastern Tianshan, northwest China: constraints from PGE geochemistry and Os–S isotopes. Ore Geol. Rev. 90, 591–606.
Mao, Y.J., Barnes, S.J., Qin, K.Z., Tang, D.M., Martin, L., Su, B., Evans, N., 2019. Rapid orthopyroxene growth induced by silica assimilation: constraints from sector-zoned orthopyroxene, olivine oxygen isotopes and trace element variations in the Huangshanxi Ni-Cu deposit, Northwest China. Contrib. Mineral. Petrol. 174, 33. https://doi.org/10.1007/s00410-019-1574-6.
Nasdala, L., Hofmeister, W., Norberg, N., Martinson, J.M., Corfu, F., Dörr, W., Kamo, S.L., Kennedy, A.K., Kronz, A., Reiners, P.W., Frei, D., Kosler, J., Wan, Y., Götze, J., Häger, T., Kröner, A., Valley, J.W., 2008. Zircon M257 - a homogeneous natural reference material for the ion microprobe U-Pb analysis of zircon. Geostand. Geoanal. Res. 32, 247–265.
Piña, R., Romeo, I., Ortega, L., Lunar, R., Capote, R., Gervilla, F., Tejero, R., Quesada, C., 2010. Origin and emplacement of the Aguablanca magmatic Ni-Cu-(PGE) sulfide deposit, SW Iberia: a multidisciplinary approach. Geol. Soc. Am. Bull. 122, 915–925.
Pirajno, F., Mao, J.W., Zhang, Z.C., Zhang, Z.H., Chai, F.M., 2008. The association of mafic–ultramafic intrusions and A-type magmatism in the Tianshan and Altay orogens, NW China: implications for geodynamic evolution and potential for the discovery of new ore deposits. J. Asia Earth Sci. 32, 165–183.
Qin, K.-Z., Su, B.-X., Sakyi, P.A., Tang, D.-M., Li, X.-H., Sun, H., Xiao, Q.-H., Liu, P.-P., 2011. SIMS zircon U-Pb geochronology and Sr-Nd isotopes of Ni-Cu-bearing mafic-ultramafic intrusions in eastern Tianshan and Beishan in correlation with flood basalts in Tarim basin (NW China): constraints on a ca. 280 Ma mantle plume. Am. J. Sci. 311, 237–260.
Ripley, E.M., Li, C., 2011. A review of conduit-related Ni-Cu-(PGE) sulfide mineralization at the Voisey's Bay Deposit, Labrador, and the Eagle Deposit, Northern Michigan. Econ. Geol. 17, 181–197.
San, J.-Z., Qin, K.-Z., Tang, Z.-L., Tang, D.-M., Su, B.-X., Sun, H., Xiao, Q.-H., Liu, P.-P., 2010. Precise zircon U-Pb age dating of two mafic-ultramafic complexes at Tulaergen large Ni-Cu districtand its geological implications. Acta Petrol. Sin. 26 (10), 3027–3035 (in Chinese with English abstract).
Seat, Z., Mary Gee, M.A., Grguric, B.A., Beresford, S.W., Grassineau, N.A., 2011. The Nebo-Babel Ni-Cu-PGE sulfide deposit (West Musgrave, Australia): Pt. 1. U/Pb Zircon ages, whole-rock and mineral chemistry, and O-Sr-Nd isotope compositions of the intrusion, with constraints on petrogenesis. Econ. Geol. 106, 527–556.
Shi, Y., Wang, Y.W., Wang, J.B., Zhao, L.T., Xie, H.J., Long, L.L., Zou, T., Li, D.D., Zhou, G.C., 2018. Physicochemical control of the Early Permian Xiangshan Fe-Ti oxide deposit in Eastern Tianshan (Xinjiang). NW China: J. Earth Sci. 29, 520–536.
Shi, Z., Chen, H.-J., Qian, Z.-Z., Xu, G., Feng, Y.-Q., Duan, J., Ren, M., 2019. Genesis and Cu-Ni metallogenetic potential of Hongshigang mafi-ultramafic intrusion in East Tianshan, China. J. Earth Sci. Environ. 41, 156–169 (in Chinese with English abstract).
Shu, L., Wang, B., Zhu, W., Gao, Z., Charvet, J., Zhang, Y., 2011. Timing of initiation of extension in the Tianshan, based on structural, geochemical and geochronological analyses of bimodal volcanism and olistostrome in the Bogda Shan, (NW China). Int. J. Earth Sci. 100, 1647–1663.

Song, X.-Y., Chen, L.-M., Deng, Y.-F., Xie, W., 2013. Syn-collisional tholeiitic magmatism induced by asthenosphere upwelling due to slab detachment at the southern margin of the Central Asian Orogenic Belt. J. Geol. Soc. 170, 941–950.
Song, X.-Y., Yi, J.-N., Chen, L.-M., She, Y.-W., Liu, C.-Z., Dang, X.-Y., Yang, Q.-A., Wu, S.-K., 2016. The giant Xiarihamu Ni-Co sulfide deposit in the East Kunlun Orogenic Belt, Northern Tibet Plateau, China. Econ. Geol. 111, 29–55.
Song, X.-Y., Wang, K.-Y., Barnes, S.J., Yi, J.-N., Chen, L.-M., Schoneveld, L.E., 2020. Petrogenetic insights of chromite in ultramafic cumulates: Implications from the Xiarihamu intrusion, northern Tibet Plateau, China. Am. Mineral. 105 (4), 479–497.
Stacey, J.S., Kramers, J.D., 1975. Approximation of Terrestrial Lead Isotope Evolution by a Two-Stage Model. Earth Planet. Sci. Lett. 26, 207–221.
Sun, T., Qian, Z.-Z., Tang, Z.-L., Jiang, C.-Y., He, K., Sun, Y.-L., Wang, J.-Z., Xia, M.-Z., 2010. Zircon U-Pb chronology, platinum group element geochemistry characteristics of Hulu Cu-Ni deposit, East Xinjiang, and its geological significance. Acta Petrol. Sin. 26, 3339–3349 (in Chinese with English abstract).
Sun, T., Qian, Z.-Z., Deng, Y.-F., Li, C., Song, X.-Y., Tang, Q.-Y., 2013a. PGE and isotope (Hf-Sr-Nd-Pb) constraints on the origin of the Huangshandong magmatic Ni-Cu sulfide deposit in the Central Asian Orogenic Belt, Northwestern China. Econ. Geol. 108, 1849–1864.
Sun, T., Qian, Z.-Z., Li, C., Xia, M.-Z., Yang, S.-H., 2013b. Petrogenesis and economic potential of the Erhongwa mafic-ultramafic intrusion in the Central Asian Orogenic Belt, NWChina: constraints from olivine chemistry, U-Pb age and Hf isotopes of zircons, and whole-rock Sr-Nd-Pb isotopes. Lithos 182-183, 185–199.
Vaillant, M.L., Barnes, S.J., Mole, D.R., Fiorentinic, M.L., Laflamme, C., Denyszyn, S.W., Austin, J., Patterson, B., Godel, B., Hicks, J., Maoa, Y.-J., Neaud, A., 2020. Multidisciplinary study of a complex magmatic system: the Savannah Ni-Cu-Co Camp, Western Australia. Ore Geol. Rev. 117, 103292.
Van Hunen, J., Allen, M.B., 2011. Continental collision and slab break-off: a comparison of 3-D numerical models with observations. Earth Planet. Sci. Lett. 302, 27–37.
Wang, B., Chen, Y., Zhan, S., Shu, L., Faure, M., Cluzel, D., Charvet, J., Laurent-Charvetd, S., 2007. Primary Carboniferous and Permian paleomagnetic results from the Yili Block (NW China) and their implications on the geodynamic evolution of Chinese Tianshan Belt. Earth Planet. Sci. Lett. 263, 288–308.
Wang, B., Cluzel, D., Jahn, B.-M., Shu, L.-S., Chen, Y., Zhai, Y., Branquet, Y., Barbanson, L., Sizaret, S., 2014. Late Paleozoic pre- and syn-kinematic plutons of the Kangguer-Huangshan shear zone: inference on the tectonic evolution of the Eastern Chinese North Tianshan. Am. J. Sci. 314, 43–79.
Wang, M.F., Guo, X., Michalak, P.P., Xia, Q., Xiao, F., Wang, W., Liu, K., 2015. Origin of the Tudun Cu-Ni sulfide deposit in the eastern Tianshan, NW China: constraints on the geochemistry of platinum group elements. Ore Geol. Rev. 64, 445–454.
Wang, Y., Lv, X., Liu, Y., 2018. Petrogenesis and Ni-Cu-Co sulfide formation of mafic enclaves in Tulaergen mafic-ultramafic intrusive rocks, Eastern Tianshan, northwest China: implications for liquid immiscibility and hydrothermal remobilization of platinum-group elements. Econ. Geol. 113, 1795–1816.
Wang, K.-Y., Song, X.-Y., Yi, J.-N., Barnes, S.J., She, Y.-W., Zheng, W.-Q., Schoneveld, L.E., 2019. Zoned orthopyroxenes in the Ni-Co sulfide ore-bearing Xiarihamu mafic-ultramafic intrusion in northern Tibetan Plateau, China: implications for multiple magma replenishments. Ore Geol. Rev. 113, 103082.
Wei, B., Wang, C.Y., Li, C., Sun, Y., 2013. Origin of PGE-depleted Ni-Cu sulfide mineralization in the Triassic Hongqiling No. 7 orthopyroxenite intrusion, Central Asian orogenic belt, northeastern China. Econ. Geol. 108, 1813–1831.
Wiedenbeck, M., Alle, P., Corfu, F., Griffin, W.L., Meier, M., Oberli, F., Vonquadt, A., Roddick, J.C., Speigel, W., 1995. Three natural zircon standards for U–Th–Pb, Lu–Hf, trace element and REE analyses. Geostand. Newslett. 19, 1–23.
Williams, I.S., 1998. U-Th-Pb geochronology by ion microprobe. Rev. Econ. Geol. 7, 1–35.
Xiao, Q.H., Qin, K.Z., Tang, D.M., Su, B.X., Sun, H., San, J.Z., Cao, M.J., Hui, W.D., 2010. Xiangshanxi composite Cu-Ni-Ti-Fe deposit belongs to comagmatic evolution product: evidences from ore microscopy, zircon U-Pb chronology and petrological geochemistry, Hami, Xinjiang, NW China. Acta Petrol. Sin. 26, 503–522 (in Chinese with English abstract).
Xiao, W.-J., Windley, B.F., Sun, S., Li, J., Huang, B., Han, C., Yuan, C., Sun, M., Chen, H., 2015. A tale of amalgamation of three Permo-Triassic collage systems in Central Asia: oroclines, sutures, and terminal accretion. Annu. Rev. Earth Planet. Sci. 43, 477–507.
Xiao, W.-J., Zheng, Y.-F., Hou, Z.-Q., Windley, B.F., Zhao, G.-C., Sun, M., Zhang, J., Song, D.-F., Zhang, H.-R., 2019. Tectonic framework and phanerozoic geologic evolution of China. Soc. Econ. Geol. Spec. Publ. 22, 21–102.
Xie, W., Song, X.-Y., Deng, Y.-F., Wang, Y.-S., Ba, D.-H., Zheng, W.-Q., Li, X.-B., 2012. Geochemistry and petrogenetic implications of a Late Devonian mafic-ultramafic intrusion at the southern margin of the Central Asian Orogenic Belt. Lithos 144, 209–230.
Xie, W., Song, X.-Y., Chen, L.-M., Deng, Y.-F., Zheng, W.-Q., Wang, Y.-S., Luan, Y., 2014. Geochemistry insights on the genesis of the subduction-related Heishan magmatic Ni-Cu-(PGE) deposit, Gansu, northwestern China, at the southern margin of the Central Asian Orogenic Belt. Econ. Geol. 109, 1563–1583.
Xue, S.-C., Li, C., Qina, K.-Z., Tang, D.-M., 2016. A non-plume model for the Permian protracted (266-286 Ma) basaltic magmatism in the Beishan–Tianshan region, Xinjiang, Western China. Lithos 256-257, 243–249.
Yang, S.-H., Zhou, M.-F., 2009. Geochemistry of the ~430-Ma Jingbulake mafic–ultramafic intrusion in Western Xinjiang, NW China: implication for subduction related magmatism in the South Tianshan orogenic belt. Lithos 113, 259–273.
Yao, J.H., Zhu, W.G., Li, C., Zhong, H., Bai, Z.J., Ripley, E.M., Li, C., 2018. Petrogenesis and ore genesis of the lengshuiqing magmatic sulfide deposit in Southwest China: constraints from chalcophile elements (PGE, Se) and Sr-Nd-Os-S isotopes. Econ. Geol. 113, 675–698.
Zhang, M.J., Li, C., Fu, P., Hu, P., Ripley, E.M., 2011. The Permian Huangshanxi Cu-Ni deposit in western China: intrusive–extrusive association, ore genesis, and exploration implications. Mineral. Deposita 46, 153–170.
Zhao, Y., Xue, C., Zhao, X., Yang, Y.Q., Ke, J., 2015. Magmatic Cu-Ni sulfide mineralization of the Huangshannan mafic-untramafic intrusion. Eastern Tianshan, China: J. Asian Earth Sci. 105, 155–172.
Zhao, Y., Xue, C.-J., Symons, D.T.A., Zhao, X.-B., Zhang, G.-Z., Yang, Y.-Q., Zu, B., 2018. Temporal variations in the mantle source beneath the Eastern Tianshan nickel belt and implications for Ni-Cu mineralization potential. Lithos 314-315, 597–616.
Zhou, M.-F., Lesher, C.M., Yang, Z.X., Li, J.W., Sun, M., 2004. Geochemistry and petrogenesis of 270 Ma Ni-Cu-(PGE) sulfide-bearing mafic intrusions in the Huangshan district, eastern Xinjiang, northwest China: implications for the tectonic evolution of the Central Asian Orogenic Belt. Chem. Geol. 209, 233–257.
Zhou, T.F., Yuan, F., Zhang, D.Y., Fan, Y., Liu, S., Peng, M.X., Zhang, J.D., 2010. Geochronology, tectonic setting and mineralization of granitoids in Jueluotage area, eastern Tianshan, Xinjiang. Acta Petrol. Sin. 26, 478–502 (in Chinese with English abstract).